Local polymer dynamics under strong connectivity constraints: The dendrimer case

K. Karatasos[a)]
Chemical Engineering Department, Aristotle University of Thessaloniki, Physical Chemistry Laboratory, 54124 Thessaloniki, Greece

A. V. Lyulin
Group Polymer Physics, Eindhoven Polymer Laboratories, Technische Universiteit Eindhoven, P.O. Box 513, 5600 MB Eindhoven, The Netherlands and Dutch Polymer Institute, Technische Universiteit Eindhoven, P.O. Box 513, 5600 MB Eindhoven, The Netherlands

(Received 21 August 2006; accepted 9 October 2006; published online 14 November 2006)

The characteristics of local motion are explored by molecular dynamics simulations in a series of AB_2-type dendrimer melts. Systems of generations 3–5 were simulated in a wide temperature range, allowing the assessment of effects associated with molecular size, proximity to the detected glasslike transitions, and the strong connectivity constraints imposed by the dendritic topology. Investigation of the mechanisms involved in local motion at short temporal and spatial scales revealed the connection between the non-Gaussian nature of monomer displacements to α-relaxation and the caging/decaging process under different degrees of confinement. In the latter mechanism, two characteristic localization lengths were identified: at the low temperature limit spatial localization was realized within approximately 10% of the nearest neighbor distance while at temperatures higher than the glass transition, the existence of an analogous length scale is ascribed to the geometric constraints due to the dense connectivity pattern. As the results from this study are discussed in comparison to the behavior observed in linear polymers and supercooled liquids, new insight is provided on the universal/specific mechanisms involved in local dynamics of different glass-forming systems. © *2006 American Institute of Physics*.
[DOI: 10.1063/1.2386155]

I. INTRODUCTION

The description of the motional mechanisms governing local polymer dynamics continues to be of great scientific interest, as it is directly associated with the understanding of glass transition phenomena and consequently with a number of important physical properties of these materials.[1] Apart from particularities associated with polymer microstructure, comparison to the characteristics of local motion in nonbonded glass-forming systems indicated that at appropriately short spatial scales connectivity effects are at a certain extent suppressed, leaving ground for a common dynamic description.

In this context, theoretical approaches developed for simple liquids such as the mode coupling theory[2] (MCT) have been successfully applied to polymeric systems as well.[3–6] At such subnanometer scale and in the dynamic range of the β-relaxation where the glass-forming units are moving within a "cage" formed by their immediate neighbors,[7–10] polymer specific effects are seemingly not directly involved. Notwithstanding, even at these very short spatial dimensions indirect effects such as the modification of local packing characteristics due to the applied intramolecular potentials in polymeric models,[4] or even correlation of motion within the cage[11,12] should properly be taken into account. At longer length scales and/or later times near the late-β/early-α dynamic range, the so-called "decaging" (i.e., escape from the cage) process takes place. In this regime, a common feature detected in liquids,[7,13] colloids,[14,15] and polymers[16,17] is the existence of mobility contrast among the glass-forming units. The observed dynamic heterogeneity is characterized by a non-Gaussian distribution in the particle/monomer displacements $r(t)$ at the relevant spatial and temporal scales, which can be quantified by means of the non-Gaussian parameter (NGP),[18]

$$\alpha_2(t) = \tfrac{3}{5}\langle[r(t)-r(0)]^4\rangle/\langle[r(t)-r(0)]^2\rangle^2 - 1. \quad (1)$$

The time t^* at which NGP exhibits a maximum demarcates a characteristic lifetime of the transient cage[7,9,19,20] and has been correlated with the time scale at which local dynamic heterogeneities approach a maximum.[10,12,20,21] At this transition region connectivity effects become increasingly important.[9,16] Instead of the free diffusion realized in simple unassociated liquids, a subdiffusive behavior is observed in monomer motion due to bonding, before final diffusion sets in.[4,6,9,16] Close examination of the motional mechanisms at this time and length scales in different kinds of glass-forming systems[9,20,22,23] revealed the key role of mobility-correlated subregions in the realization of cooperative motion. In the case of polymers chain connectivity may provide alternative routes, not present in simple liquids, for short range spatially correlated dynamics.[6,16,24]

[a)]Author to whom correspondence should be addressed. Electronic mail: karatas@eng.auth.gr

In this work we aim at a closer view on those mechanisms governing local polymer motion under a dense connectivity pattern and a well defined mobility contrast, by examining polymeric models bearing the dendritic topology. Dendrimers are glass-forming polymeric materials[25–28] with a quantitatively described level of dynamic heterogeneity well localized within their structure.[27–31] These attributes may essentially "filter out" certain dynamic features met either in liquids or linear polymers allowing a better assessment of the relative importance of each factor. For instance, in both of these glass-forming systems, regions of low or high mobility may fluctuate through the sample in a finite time scale, promoting specific mechanisms for cooperative particle rearrangements (e.g., stringlike particle/monomer clusters[9,22]) that are expected to be suppressed in dendrimers. Identification and monitoring of regions possessing distinct mobilities rely on a proper selection of subensembles of "fast" and "slow" moving units, for the definition of which various approaches have been followed so far.[6,19,32,33] This introduces a freedom that might be undesirable when it comes to comparison of results obtained from different such selections. In the case of dendrimers, the sets of beads belonging to different generational shells (*g shells*, see next section) form ideal subensembles for the elucidation of mobility contrast effects in the realization of local motion, particularly in the proximity of glass transition phenomena.[28] On the other hand, the effects of strong connectivity constraints on the character of local cooperative motion can be naturally explored due to their highly branched topology.

To this end we have conducted molecular dynamics (MD) simulations in a series of model dendrimers in the melt, at a wide temperature range covering regions of both high and low monomer mobilities. The principal aim of this work is to explore the impact of a connectivity-controlled constricted environment, to the mechanisms involved in local structural relaxation at different temperature distances from the glass transition. In this context, the relation between the detected non-Gaussianity in monomer motion to the caging/decaging process as well as to the α-relaxation and the manifestation of glass transition phenomena are discussed in detail.

The organization of the paper is as follows: in Sec. II a brief description is given for the models and the simulation method utilized. Section III discusses the non-Gaussianity of local motion at distinct temperature regions and different levels of confinement, and its relation to the early stages of α-relaxation. Characterization of the spatial scale of monomer localization at various distances from T_g is provided in Sec. IV, while in Sec. V dynamic aspects of the caging/decaging process are explored. Finally, the main characteristics of the observed behavior and the conclusions drawn are summarized in Sec. VI.

II. MODEL AND SIMULATION DETAILS

The dendrimer molecules were modeled in the united atom (UA) representation starting from a trifunctional core, bearing branching functionality equal to 3 and two spacer bonds between branching points as schematically depicted in Fig. 1. The concentric circles in the schematic denote the different generational shells g. The maximum number of shells defines the generation G of the dendrimer. Systems of generations $G=3$ to $G=5$ were simulated by means of molecular dynamics simulations in the bulk state under the constant-temperature, constant-pressure (NPT) thermodynamic ensemble,[34] at temperatures ranging between 750 and 350 K and between 800 and 350 K for the G3, G4, and G5 systems, respectively. Melts of G3 and G4 models were comprised by 30 and G5 systems by 25 molecules. According to the adopted topology the number of beads as a function of the generational shell index g (starting from 0) is given by $N(g)=1+6[2^{g+1}-1]$, yielding systems consisted of $30\times N(3)=2730$, $30\times N(4)=5610$, and $25\times N(5)=9475$ united atoms for systems of generations 3, 4, and 5, respectively. The interaction potential consisted of bonded (bond stretching, bending angles, and torsions) and nonbonded (Lennard-Jones-type) terms, following the parametrization of the DREIDING force field.[35] A full description of the set of parameters, as well as details of the adopted simulation protocol (generation of the initial structures, procedure for equilibration of the melts, etc.) can be found in Refs. 27 and 28 (henceforth R1 and R2, respectively).

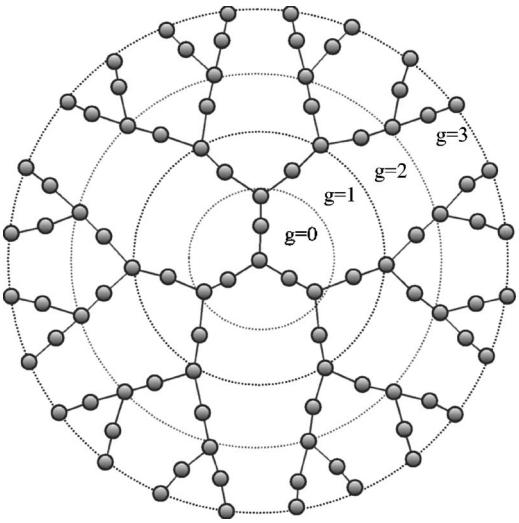

FIG. 1. Schematic representation of a dendrimer model of the third generation (G3). The concentric circles indicate the boundaries of the different generational shells (g shells).

III. NON-GAUSSIANITY AND LOCAL RELAXATION

As shown in R1 and R2, local dynamics of dendrimers is characterized by a topology-driven strong mobility contrast between beads belonging to different g shells, which is augmented upon decrease of temperature or increase of molecular weight. As the size of the dendrimer grows, the relevant time scales for motion of beads in separate g shells shift further apart, to a point where distinct freezing-in times within a dendrimer can be realized. This scenario can account for the two glasslike transitions as predicted from simulations in the larger size model[28] and as verified from recent experiments.[26] Approximate values for the glass transition temperatures (T_g) of the examined models as detected in R2 are $T_g(\mathrm{G3})\simeq 500$ K, $T_g(\mathrm{G4})\simeq 550$ K, $T_g^H(\mathrm{G5})\simeq 650$,

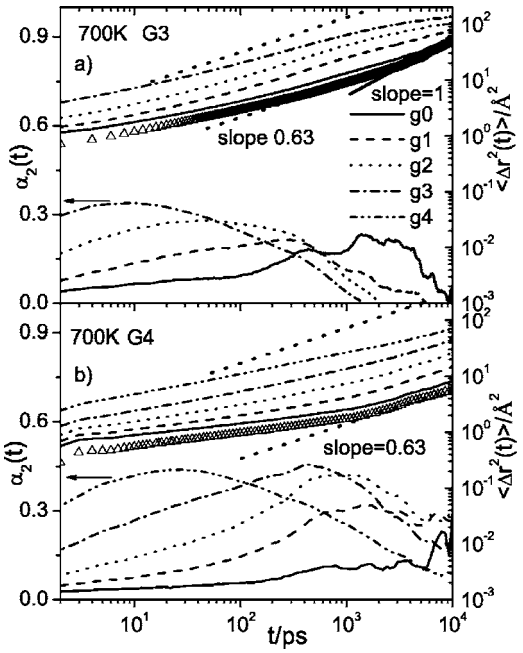

FIG. 2. Non-Gaussian parameter (left axes) and MSD (right axes) of beads belonging to different g shells at 700 K. (a) G3 model and (b) G4 model. The lines of slopes 1 and 0.63 denote the linear and the sublinear diffusive regimes. The symbols represent the MSD of the center of mass for each model.

K and $T_g^L(\mathrm{G5}) \simeq 450$ K, where T_g^H and T_g^L refer to the "high" and the "low" temperature T_g's of the largest generation system.

In R2 the degree of mobility contrast between different generations was estimated by means of ratios of the mean squared displacements (MSDs) of beads belonging to neighboring g shells. It was demonstrated that the peak shape of the mobility ratios as a function of time as well as the location of the observed maxima could be rationalized by the fact that decaging of beads in different generational shells was taking place at distinct time scales. The inner the g shell, the longer the time scale for the escape of the beads from their cage. In addition, increase of molecular size resulted to longer decaging times.

Figures 2(a) and 2(b) show the time dependence of the NGP and the MSD of beads belonging to different g shells, for the G3 and the G4 models, at a temperature $T=700$ K, above the respective T_g's. At constant dendrimer size, the NGP appears to shift the location of its maximum to longer times, while at the same time assumes lower values the inner the g shell is located within the dendritic structure. Comparison of the behavior of the NGP between the two models at g shells equidistant from the surface indicates an overall increase of the NGP and a shift of its maximum to larger time scales as the size of the model grows. Considering the correlation of the temporal scale of the NGP maxima to the characteristic time for the decaging process, we can already single out two factors that appear to be decisive for the determination of characteristic time scales for local bead motion: the relative location of the beads within the dendritic structure as can be expressed by the generational shell index, and the size of the dendrimer they belong in.

Valuable information can also be extracted from the behavior of the corresponding MSDs. For both systems, apart from the squared displacements of beads at different g shells, the center of mass behavior is included in the plot. Focusing on the smaller size model (Fig. 2), two regimes can be distinguished in the center of mass motion at longer times: (i) at the longest examined time scales the center of mass has reached the long-range diffusive limit as indicated by the proportionality between MSD and time, and (ii) at shorter times a subdiffusive regime can be identified, with a slope indistinguishable from 0.63 which is the power law observed in the MSD of interior beads in linear chain models prior to the crossover to free diffusion.[4,6,16] Regime (ii) is preceded by a regime where the MSD is an even weaker function of time, corresponding to the "caged" motion in analogy to the behavior observed in the MSD of the center of mass of linear polymers and colloids.[6,15] It worths noticing that a similar behavior is only followed by beads residing in the innermost g shell ($g0$), while beads at the outer g shells appear to move subdiffusively even at the long-time limit of the examined dynamic range. An analogous behavior is observed in the MSDs of beads in distinct g shells at the G4 dendrimer, with one difference: no free-diffusion regime is present for the center of mass or for the innermost g shell in the examined window. This is expected to be shifted to longer time scales due to the increased molecular size. The same tendencies characterize the behavior of the G5 dendrimers as well.

A visual inspection of the NGPs in both models reveals that peak positions particularly for the outer g shells are located at time scales well within the subdiffusive regime, rather far apart from the transition region to the diffusive behavior. The time window for subdiffusive motion particularly for the larger model studied extends to several decades following a power law $\langle \Delta r^2(t) \rangle \propto t^{\delta}$ with an exponent $\delta < 0.63$. This notion holds true for the outer g shell behavior, even at the time scales at which the center of mass attains the diffusive limit. For the larger generation system G5 (not shown here) this behavior is more prominent. Such a persistence of sublinear diffusion over very long time scales has previously been observed in disordered media models and has been attributed to mode coupling effects that essentially enhance cooperativity of motion,[33] or to diffusion in a subvolume of fractal dimensions.[36,37] Both of these interpretations represent plausible scenaria for motion of dendrimer beads, since it takes place in a microenvironment that bears fractal characteristics[38] and under a strong connectivity pattern that enhances cooperativity of motion.

The relation between the MSD and the associated NGP arising from beads' motion at a specific g shell differentiates in several aspects when compared to the behavior exhibited in linear polymers. For instance, in a linear polymer model it was noted[17] that $\alpha_2(t) \to 0$ at a time for which $\langle r^2(t) \rangle$ approaches the square value of the average intermacromolecular distance $d \simeq 2\pi/Q_{\max}$ where $Q_{\max}$ is the magnitude of the scattering vector at the first ("intermolecular") peak of the static structure factor. The value of $Q_{\max}$ for all the dendrimer models examined here amounted to[28] $Q\,\max \simeq 1.4$ Å^{-1}, yielding thus a value of $(2\pi/Q_{\max})^2 \simeq 20.1$ Å^2. As can readily be inferred from Figs. 2(a) and 2(b) at the root MSD corresponding to that Q value, with the possible excep-

tion of the interior g shell, the NGP remains well above 0. Furthermore, an attempt to draw an analogy in terms of the relative "freedom" in motion between beads of the exterior g shell and those of the interior g shells with the end beads and the inner monomers of a polymer chain, respectively, would lead to a failure in the reproduction of linear models' behavior. As was demonstrated in relevant simulation studies,[6] the ratio of the MSD of the end beads over that of the interior monomers deviates positively from unity, only at times $t > t^*$ when $\alpha_2(t)$ assumes very low values and the MSD of the interior beads scales as $\langle \Delta r^2(t) \rangle \propto t^{0.63}$. Apparently this is not the case for dendrimers, since the MSD of the outer g shell remains always significantly larger than that of any other g shell or that of the center of mass, throughout the subdiffusive regime.

The above picture describes the behavior of all the examined models at temperatures higher than the intervention of any freezing-in event. To check the dynamic effects induced by the proximity to the glass transition region, we have followed the temperature dependence of the MSD and the NGP of all the examined systems. To draw statistically more reliable conclusions we relied to a large extent to the behavior of the beads belonging to the outer g shells of the dendrimers, since they are comprised by more than half of the united atom population per molecule. Figures 3(a)–3(c) portray the time and temperature dependence of the MSD and the NGP for the exterior g shells for dendrimers of generations 3, 4, and 5, respectively. The points denote the peak locations of the NGPs, while the lines through them are guides for the eye. Each line goes through a different group of temperatures as they were defined from static and dynamic processes in R2 (i.e., two lines—one T_g—for G3 and G4 dendrimers and three lines—two T_g's—for the G5 system). According to the procedures followed for the determination of these regimes (i.e., temperature dependence of the specific volume and temperature dependence of bond relaxation rates) a change from one regime to another signifies a glasslike transition. Evidently, the temperature dependencies of the maxima of the NGPs for all models result to changes in slopes which agree with those utilized for the determination of the nominal glass transitions.[28] In other words, the dynamic slowdown of local motion in the vicinity of glass transition and the ensuing freezing-in events appear to be imprinted in the behavior of the non-Gaussian parameter. Associations of the temporal scale t^* at which the NGP peaks with the time scale for collective motion responsible for the α-relaxation process have already been noticed in different glass-forming systems. Studies in supercooled liquids[13,19,22] demonstrated the relation of t^* with the lifetime of the dynamic heterogeneities and the cooperative motion necessary for the release of the particles from their cage, which characterizes the early stages of α-relaxation. In linear polymer models it was shown[6,9] that NGP peaks in the late-β/early-α regime, while t^* was found to follow a similar temperature dependence with that of the α-relaxation (see Ref. 39 and references therein).

In our previous works R1, R2 local dynamics pertinent to the α-relaxation mechanism was monitored by means of the second order bond reorientation correlation function

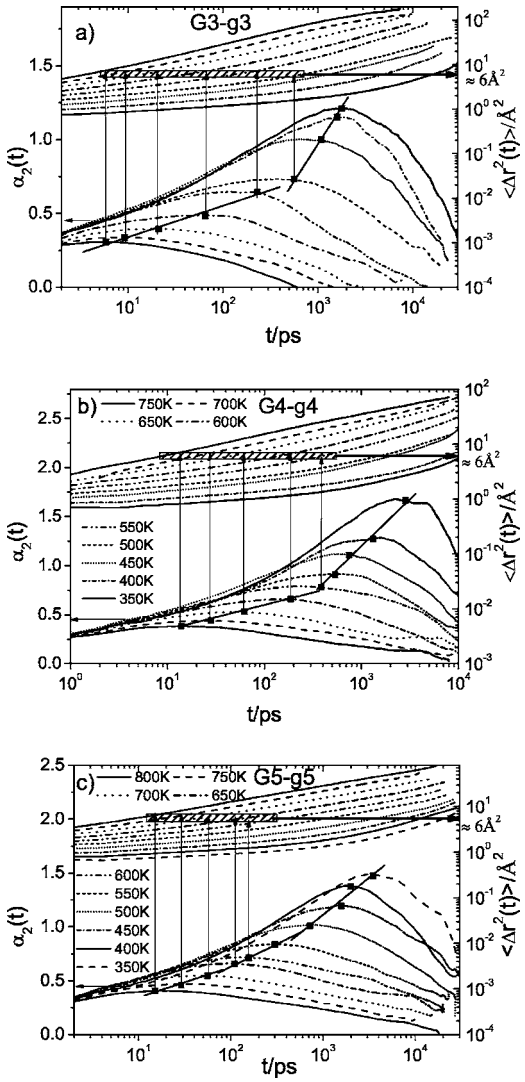

FIG. 3. Temperature dependence of the NGP and MSD of the outer g shells (a) G3-g3, (b) G4-g4, and (c) G5-g5. Assignment of the curves to corresponding temperatures in (a) is the same as in (b). The thick solid lines denote the different temperature regimes as determined in R2 (see text). The points indicate the peak positions of the respective NGPs. The vertical arrows intersect the MSD curves at the time location of the NGP maxima. The hatched areas represent a margin within which the intersections of the arrows with the relevant MSD curves reside. The long horizontal arrows point at the average MSD value corresponding to the hatched area.

$P_2(t) = \frac{1}{2}\langle 3[\hat{h}(t)\cdot\hat{h}(0)]^2 - 1 \rangle$ ($\hat{h}$ symbolizes the unit vector along an examined bond). Analysis of the obtained spectra was based on the calculation of the distribution of relaxation times (DRT),[40] according to which dynamic correlation functions are described as a continuous superposition of single exponential processes with a distribution function $F(\ln \tau)$. In this representation dynamic processes well separated in time scale appear as distinct peaks in the distributions, while positions of the maxima provide a good estimation of their characteristic times in the case of symmetric peaks. This analysis allowed the identification of the different motional mechanisms involved in local scale dynamics and provided information on their relative contribution as the systems were approaching structural/motional arrest.

The relaxation mode which exhibited the more sensitive response to temperature variations in terms of changes in

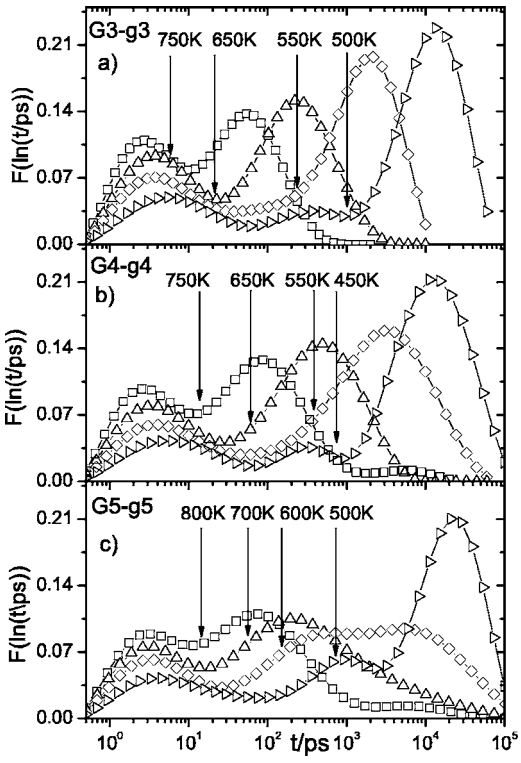

FIG. 4. Distribution of relaxation times from analysis of bond reorientational spectra (see text) from the exterior g shells at temperatures above and below the respective T_g's: (a) G3-g3, (b) G4-g4, and (c) G5-g5. Abscissas of the vertical arrows correspond to the time locations of the respective NGP maxima.

amplitude and characteristic time was the slower process, which contributed the most to the determination of the average relaxation time[28] and thus to the α-like character of bond reorientation. Figure 4 shows the peak locations of the NGPs relative to the DRTs at different temperatures representing regimes above as well as below the estimated glass transition temperatures for the outer g shells of the examined models. Clearly at temperatures higher than the respective T_g's and for all the dendrimer systems, the maxima t^* of the respective NGPs are located at the onset of the slower process which essentially traces the α-relaxation behavior as discussed before. At temperatures below the T_g of the smaller size models and the T_g^H of the G5 system, t^* either retains the same relative position or corresponds to the time scale of the intermediate process which in any case is very close to that of the slower mode. This low-amplitude peak appearing below T_g at a slightly shorter characteristic time presumably originates from a faster moving bond population near the dendrimer periphery as is discussed in R2. The same picture was found to describe the behavior of the inner generational shells as well, at least for those g shells that were possible to obtain at the same time a sufficient degree of $P_2(t)$ decorrelation and a well defined maximum of the NGP.

In light of these observations, a direct connection between the maximum degree of non-Gaussianity in local motion and the release from the cage, which signifies the early stage of α-relaxation, is in order. It is noteworthy that the onset of the slow process resides well within the subdiffusive regime and several decades earlier than final diffusion, since no diffusive regime can be detected in the MSD of the outer generational shells in the examined time windows.

IV. CAGED MOTION AND LOCALIZATION LENGTH

The MSD at the maximum of the NGP $\langle \Delta r^2(t^*) \rangle$ has been associated in polymeric models[9,17,41,42] with a characteristic spatial dimension r_{sc} for transient particle localization $\langle \Delta r^2(t^*) \rangle \sim 6r_{sc}^2$. Suggested microscopic pictures involve particle confinement to rather uniform cages of neighboring particles at times $t \ll t^*$ while at times $t \gg t^*$ accumulated individual displacement steps result to a regular diffusive motion.[39] In the case of glass-forming liquids similar mechanisms assuming spatially correlated motion in localized dimensions have also been described.[12,43] As is pointed out in Figs. 3(a)–3(c) by arrows, at temperatures *above* the estimated T_g's and for all the examined models $\langle \Delta r^2(t^*) \rangle$ assumes (within a small margin indicated by the hatched areas) an almost constant value of ≈ 6 Å^2. At temperatures lower than the glass transition, however, $\langle \Delta r^2(t^*) \rangle$ starts to deviate [arrow ends at $T < T_g$ in Figs. 3(a)–3(c) lie below the hatched area] from the high temperature behavior.

To further elucidate the nature of monomer motion at the time scale where the NGP is maximized we have calculated the distribution of the bead displacements belonging to the exterior g shell at $t=t^*$, $P(r;t^*)$ for all the examined models. Comparison of the distributions of the bead displacements at temperatures above the respective T_g's (not shown here) indicated that for each dendrimer model, the distributions at the examined temperature range practically overlap, implying that not only the average values $\sqrt{\langle \Delta r^2(t^*) \rangle} \approx \sqrt{6}$ Å at these temperatures are comparable, but also that the effective local microenvironments share common characteristics. At temperatures close or moderately below the glass transition, as one might have already suspected from Fig. 3 the superposition of distributions fails. This failure attests to the dependence of the local environment characteristics on temperature and molecular weight. To check for such effects, we have calculated the distributions at all the examined temperatures at $t=t^*$ for each model and collated their characteristics. Figures 5(a)–5(c) compare the histograms corresponding to the outer g shells at three different temperatures representing states below, at the vicinity, and above the glass transition (for the G5 model only the higher temperature is above the T_g^H).

At the temperature which lies above their respective T_g's the distributions are practically superimposed, at the intermediate temperature no collapse of the curves is observed, while at the lowest temperature the superposition is restored. To obtain an overview of this behavior we have utilized as a probe the length scale representing the average bead displacement at $t=t^*$ since it is closely associated with the dimensions of the spatial localization of motion. In this manner we were able to map the response of the corresponding microenvironments as a function of the relative distance from the glass transition and as a function of molecular size of the models. This length scale r^* was determined by means of the calculated distributions according to

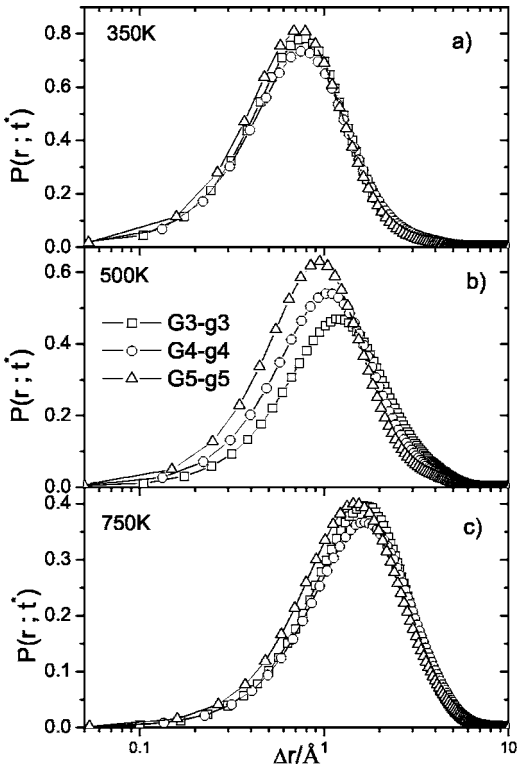

FIG. 5. Comparison of distributions of bead displacements for G3-g3, G4-g4, and G5-g5 shells at $t=t^*$ and at temperatures below (a), close (b), and above (c) the respective T_g's.

$$r^* = \int_0^{r_{\max}} P(r;t^*) r dr \Big/ \int_0^{r_{\max}} P(r;t^*) dr,$$

where $r_{\max}$ is defined by $P(r>r_{\max};t^*)=0$.

The temperature and model-size dependence of r^* are mapped in Fig. 6. At the high temperature regime r^* seems to converge for all the models to a value of $r^* \simeq 2.25$ Å, in close agreement to the graphically estimated value of $\sqrt{6}$ Å from Figs. 3(a)–3(c). At a temperature close to the glass transition of each model (for the G5 close to the "high temperature" T_g^H) r^* begins to decrease monotonically towards a low temperature limit of $r^* \simeq 1.20$ Å. The fact that at the two limiting cases r^* appears within the calculation margins to be independent from the size of the models, combined with the observed collapse of the corresponding distributions, implies the existence of generic mechanisms in local motion at these limits. At the intermediate temperature regime, however, a model-size-dependent behavior is observed. As a general remark we notice a tendency for lower r^* values upon increase of the dendrimer size. On the other hand, while for the lower size models a change in slope is rather prominent close to the glass transition, for the larger size model at $T<T_g^H$ the curve undergoes a smooth change of slope passing through T_g^L as the low temperature limit of r^* is approached. In the past studies in linear polymers,[17] it was noted that the mean localization length r_{sc} calculated from $\Delta r^2(t^*) \sim 6r_{sc}^2$, when expressed in terms of the intermolecular distance $d=2\pi/Q_{\max}$ ($Q_{\max}$ represents the magnitude of the first peak of the static structure factor) it yields a value of $r_{sc}/d \simeq 0.094$ very close to a value of 0.095 that was also found in linear bead-spring models.[9,41,42] A similar estimation of the mean localization length based on the value of r^* as calculated from the present models at the low temperature limit results to a value of $r_{sc}/d \simeq 0.109$ nearly identical to the Lindemann criterion for melting.[44]

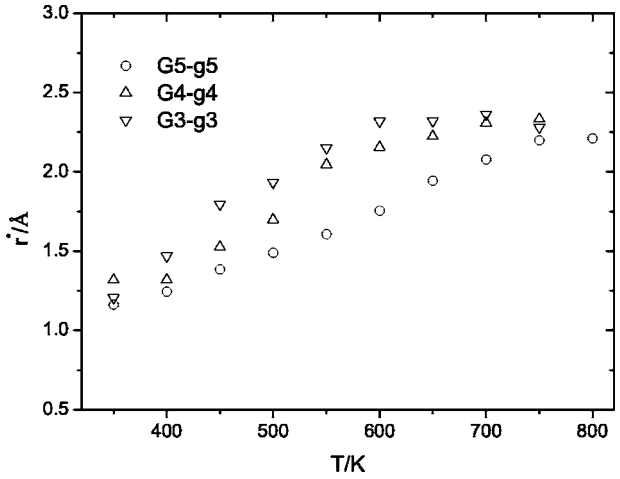

FIG. 6. Mean localization length r^* (see text) of beads belonging to the outer g shells G3-g3, G4-g4, and G5-g5 as a function of temperature.

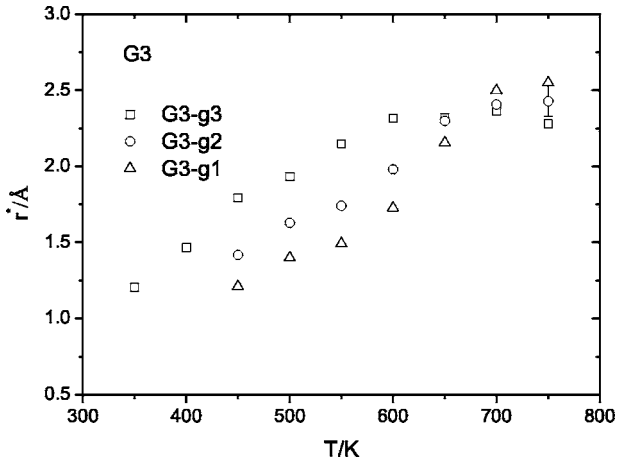

FIG. 7. Mean localization length r^* for beads belonging to different generational shells of the G3 model as a function of temperature.

To examine the dependence of r^* on the location of the beads within the dendrimer structure for a constant dendrimer size, we followed the procedure described above for the $g=1$ and $g=2$ shells of the G3 model at all the temperatures for which reliable estimations could be performed. For the larger models due to the worsening of the statistics, NGP for interior g shells was not a smooth function of time and the determination of t^* was not a well defined procedure. Therefore we avoided to draw any conclusions based on these models. As shown in Fig. 7 for the G3 model, while the estimated high temperature limits for r^* were within the error margins similar to those calculated for the outer g shell, at intermediate temperatures inner g shells exhibited (beyond the error) smaller r^* values indicating a shorter localization length.

On these accounts, rationalization of the low and the high temperature limits of r^* is in order. The low temperature limit reflects a motion localized in spatial dimensions of the

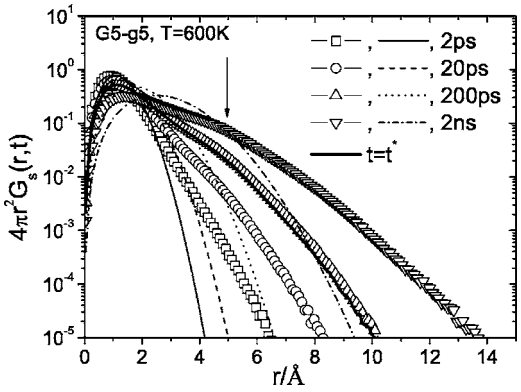

FIG. 8. Time evolution of $4\pi r^2 G_s(r,t)$ at $T=600$ K for the outer g shell of the G5 dendrimer. $G_s(r,t)$ is the self-part of the Van Hove function of the examined beads. The thick solid line denotes $4\pi r^2 G_s(r,t^*)$. The thin lines represent the corresponding Gaussian approximations. The vertical arrow indicates the location of a "bump" (see text) in the $t=2$ ns curve. The size of the error bars is approximately twice the size of the symbols for distances $r<2$ Å and about equal or smaller than the size of the symbols for longer distances.

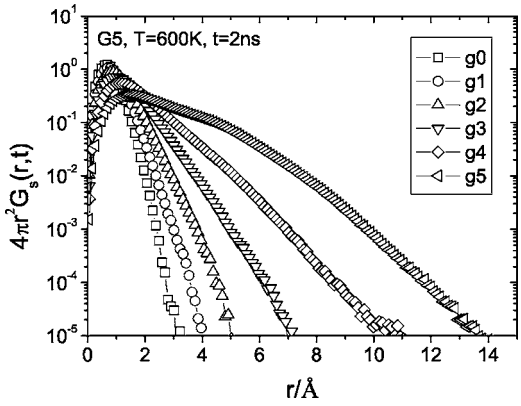

FIG. 9. $4\pi r^2 G_s(r,t)$ at $T=600$ K and $t=2$ ns of the different g shells in the G5 model. The size of the error bars is described in the caption of Fig. 8.

order of 10% of the nearest neighbor distance, above which a "melting" (i.e., a significant increase in amplitude of particle displacements) takes place. The origin for the high temperature r^* limit could be related to connectivity effects due to the dense branching pattern characterizing the dendritic structure. To the authors' knowledge no such high-temperature length scale for local motion has been identified so far in linear polymers or in other glass-forming systems.

V. DYNAMIC ASPECTS OF CAGE FORMATION

As was shown in the preceding paragraphs, the degree of localization in bead motion depends on the size of the model, on temperature, and on the relative position of the beads within the dendrimer structure. Another relevant parameter is time, in the sense of the temporal evolution of this localization/release process, which can be followed by monitoring the self-part of the Van Hove correlation function $G_s(r,t)$

$$G_s(r,t)=\frac{1}{N}\left\langle \sum_{i=1}^{N} \delta(r-|\mathbf{r_i}(0)-\mathbf{r_i}(t)|)\right\rangle .$$

N refers to the number of the particles and $\mathbf{r_i}(t)$ is the position vector of the ith particle at time t. Here the isotropic form is used. This function is proportional to the probability of finding a particle at time t at a distance r from its original position (at $t=0$), and has been successfully utilized for probing the time scale of dynamic heterogeneities and/or the time development of the decaging process.[45,46] Figure 8 shows $4\pi r^2 G_s(r,t)$ (after angular integration) at different times, for the outer g shell of the G5 dendrimer at a temperature close to the T_g^H of that model. The lines represent the Gaussian approximation[47] $4\pi r^2 G_s^G(r,t)$ where

$$G_s^G(r,t)\approx\left[\frac{3}{2\pi\langle\Delta r^2(t)\rangle}\right]^{3/2}\exp\left[-\frac{3r^2}{2\langle\Delta r^2(t)\rangle}\right].$$

Apparently, even at the shortest times examined, the Gaussian approximation fails to account for the observed $4\pi r^2 G_s(r,t)$ behavior. The effect of the increase of the time interval is to broaden the distributions shifting their tails at larger displacements. Evolution of these curves manifests the relative contribution of particle displacements to the formation of the cage at times $t\ll t^*$ and to its concomitant decay at much longer time scales.[45] It is noticeable that a bump appears in the distributions at times longer than t^* as pointed out by the arrow. This feature implies the formation of distinct populations of beads, one corresponding to beads that still remain close to their original positions after the examined time interval, and another increasing population of beads that assume larger displacements escaping thus from the cage. This bump in the distributions is actually suppressed in inner g shells for a number of possible reasons: to begin with, beads of the outer generation possess a higher probability to reside at the periphery and therefore to assume a less hindered motion that would allow displacements of larger amplitude. On the other hand, the backfolding effect works in the opposite direction since it contributes to the formation of a bead population which explores a more constricted environment. Finally, the outer g shell is comprised by more than half of the dendrimer's beads, which renders it statistically more probable that a percentage of these beads will undergo larger overall displacements.

At a time scale at which decay of the cage of the outer g shell beads has already progressed, beads residing at inner g shells are still undergoing a localized motion as shown in Fig. 9. The inner the g shell, the higher the percentage of beads that remain close to their original positions. The distributions appearing in Figs. 8 and 9 exhibit several common attributes. For instance, the distributions describing the $G_s(r,t)$ of the $g=5$ shell at $t=2$ ps and $t=200$ ps (Fig. 8) bear strong similarities with the distributions of the $g=3$ and the $g=4$ shell at $t=2$ ns (Fig. 9), respectively. This occurrence implies an "equivalence" between elapsed time and degree of confinement as far as it concerns the mechanism responsible for the escape of the cage. In other words it appears that beads belonging to different g shells will follow a similar mechanism for their decaging, but at different time scales. To a certain extent the alleged "equivalence" can also be noted when the effects of temperature and/or molecular weight are considered.

Figure 10(a) shows the temperature dependence of

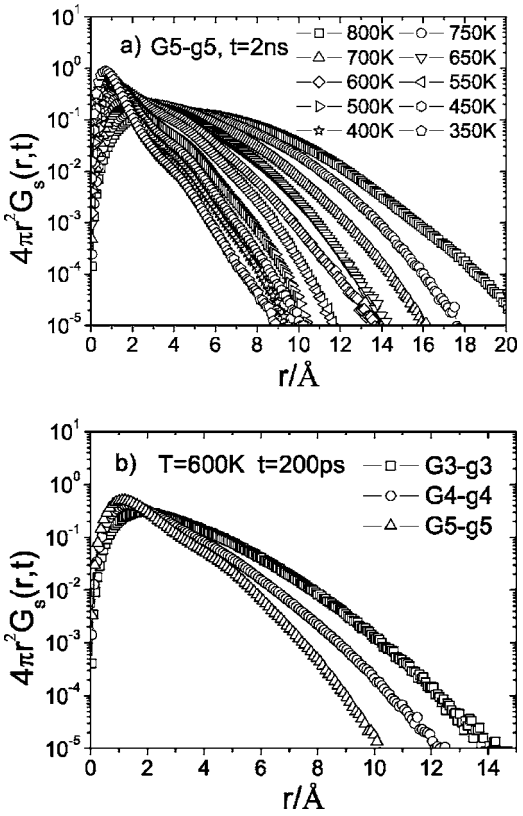

FIG. 10. (a) $4\pi r^2 G_s(r,t^*)$ of G5-g5 shell at different temperatures and at time $t=2$ ns. (b) Comparison of the behavior of self-Van Hove functions of beads belonging to the outer g shells of different size systems, at $t=200$ ps. The size of the error bars is described in the caption of Fig. 8.

$G_s(r,t)$ of the outer g shell of the G5 model at $t=2$ ns, while Fig. 10(b) compares the distributions of the exterior g shells of the examined models at constant temperature and time. Collation, e.g., between the distribution at $T=500$ K and $t=2$ ns in Fig. 10(a) and the distribution of the same g shell at $T=600$ K and $t=200$ ps in Fig. 8 corroborates the above argument. An analogous comparison can be performed, for instance, between the G3-g3 shell at $T=600$ K and $t=200$ ps [Fig. 10(b)] and the G5-g5 shell at $T=600$ K and $t=2$ ns (Fig. 8). (The bump at about 5 Å does not appear in the G3-g3 distribution since $T=600$ K lies above the respective T_g for this model.)

VI. SUMMARY/CONCLUSIONS

Examination of the degree of confinement as this is determined from the relative location of the beads within the dendritic structure and the size of the dendrimer molecule demonstrated the role of strong connectivity constraints to the mechanisms involved in realization of local motion at short spatial and temporal scales. The non-Gaussian nature of bead displacements in the subdiffusive regime was found to depend on the level of constraint: the more constricted the motion (i.e., the smaller the g shell index), the lower the NGP (Fig. 2). The extent of the time window in which dendrimer beads undergo subdiffusive motion is related to the g shell index as well: the outer the generational shell, the longer the period of the sublinear diffusion. The longer range of the subdiffusive regime in dendrimers compared to the linear polymer behavior can be rationalized by the enhanced cooperativity in local dynamics due to the dense connectivity pattern and/or by the fact that short scale motion is realized in a local environment that bears fractal characteristics. It is conjectured that for the same reasons, in contrast to the linear polymer behavior, NGP in dendrimers remains well above 0 (particularly for the outer g shells) even at time scales at which MSD exceeds the square value of the first-neighbor distance.

A common attribute that characterizes short scale motion in both dendrimers and linear models is the scaling exponent of ~0.63 which describes the MSD as a function of time at the transitional region of the late-β/early-α process. This feature can be attributed to the intervention of connectivity since it is not observed in simple nonassociated liquids. At this regime, it was found that the characteristic time t^* at which NGP assumes its peak value marks the onset of a slow dynamic mode which bears characteristics of the α-relaxation process observed in glass-forming systems. Temperature dependence of t^* seems to follow that of the bond-reorientation relaxation time which traces the dynamic slowdown in the vicinity of glass transition phenomena. As t^* is associated with the time scale for the escape of the beads from the transient cage formed by their neighbors, the connection between the decaging process and the realization of the early stages of α-relaxation is verified.

Characteristics of spatial localization of bead motion were found to depend on the distance from the glass temperatures, the degree of confinement, and the size of the dendrimer models. The lower the level of confinement (i.e., the outer the g shell or the smaller the size of the model) the larger the characteristic length scale of localization. At temperatures well above, or well below the respective T_g's, however, a limiting behavior of this spatial dimension has been observed together with a marked similarity in the relevant distributions of the bead displacements. At the low temperature limit, a molecular-size-independent value was estimated to be very close to the Lindemann criterion of melting, which is at approximately 10% of the average first-neighbor distance, in consensus with the value observed in polymer models or other glass-forming systems. At the high temperature limit a length scale close to 2.25 Å was identified, insensitive to the molecular size and the g-shell index, alluding to a mechanism driven by the dendritic branching topology. Examination of the mechanisms involved in the formation/decay of the cage, as far as it concerns the relative population of beads participating in these processes at different time scales, showed that for similar degrees of confinement in bead motion as can be determined by the g shell index for constant dendrimer size, the molecular weight of the model, and the elapsed time, similar stages are followed in this procedure.

To recapitulate, in this work we have investigated aspects of local polymer dynamics under the influence of a strongly branched environment. Similarities to the behavior of supercooled liquids and linear polymers have been pointed out, allowing a better understanding of some common features met in all of these glass-forming systems. Moreover, effects related to connectivity were identified and

the dendrimer-relevant characteristics in local motion were compared to those of linear polymeric systems, allowing an assessment of the different factors that may influence the observed behavior.

ACKNOWLEDGMENTS

Funding from the Greek General Secretariat for Research and Technology under the framework of the PENED 2003 program is gratefully acknowledged. Part of this work was carried out under the HPC-EUROPA project (RII3-CT-2003-506079), with the support of the European Community—Research Infrastructure Action under the FP6 "Structuring the European Research Area" Programme.

[1] M. Ediger, Annu. Rev. Phys. Chem. **51**, 99 (2000).
[2] W. Götze and L. Sjögren, Chem. Phys. **212**, 47 (1996).
[3] K. Binder, J. Non-Cryst. Solids **274**, 332 (2000).
[4] W. Paul and G. Smith, Rep. Prog. Phys. **67**, 1117 (2004).
[5] A. V. Lyulin, N. K. Balabaev, and M. A. J. Michels, Macromolecules **35**, 9595 (2002).
[6] J. Baschnagel and F. Varnik, J. Phys.: Condens. Matter **17**, R851 (2005).
[7] W. Kob and H. C. Andersen, Phys. Rev. E **51**, 4626 (1995).
[8] F. Sciortino, P. Gallo, P. Tartaglia, and S. H. Chen, Phys. Rev. E **54**, 6331 (1996).
[9] M. Aichele, Y. Gebremichael, F. W. Starr, J. Baschnagel, and S. C. Glotzer, J. Chem. Phys. **119**, 5290 (2003).
[10] E. Flenner and G. Szamel, Phys. Rev. E **72**, 031508 (2005).
[11] C. Bennemann, C. Donati, J. Baschnagel, and S. C. Glotzer, Nature (London) **399**, 246 (1999).
[12] S. C. Glotzer, J. Non-Cryst. Solids **274**, 342 (2000).
[13] W. Kob, C. Donati, S. J. Plimpton, P. H. Poole, and S. C. Glotzer, Phys. Rev. Lett. **79**, 2827 (1997).
[14] E. R. Weeks, J. Crocker, A. Levitt, A. B. Schofield, and D. A. Weitz, Science **287**, 627 (2000).
[15] E. R. Weeks and D. A. Weitz, Phys. Rev. Lett. **89**, 095704 (2002).
[16] J. Baschnagel, C. Bennemann, W. Paul, and K. Binder, J. Phys.: Condens. Matter **12**, 6365 (2000).
[17] J. Colmenero, F. Alvarez, and A. Arbe, Phys. Rev. E **65**, 041804 (2002).
[18] J. Boon and S. Yip, *Molecular Hydrodynamics* (Dover, New York, 1980).
[19] C. Donati, S. C. Glotzer, P. H. Poole, W. Kob, and S. J. Plimpton, Phys. Rev. E **60**, 3107 (1999).
[20] V. Teboul, A. Monteil, L. C. Fai, A. Kerrache, and S. Maabou, Eur. Phys. J. B **40**, 49 (2004).
[21] G. A. Appignanesi, M. A. Frechero, and R. A. Montani, Physica A **329**, 41 (2003).
[22] C. Donati, F. F. Douglas, W. Kob, S. J. Plimpton, P. H. Poole, and S. C. Glotzer, Phys. Rev. Lett. **80**, 2338 (1998).
[23] A. H. Marcus, J. Schofield, and S. A. Rice, Phys. Rev. E **60**, 5725 (1999).
[24] Y. Gebremichael, T. B. Schroder, F. W. Starr, and S. C. Glotzer, Phys. Rev. E **6405**, 051503 (2001).
[25] J. K. Kruger, M. Veith, R. Elsasser, W. Manglkammer, A. Le Coutre, J. Baller, and M. Henkel, Ferroelectrics **259**, 27 (2001).
[26] N. N. Smirnova, O. V. Stepanova, T. A. Bykova, A. V. Markin, A. M. Muzafarov, E. A. Tatarinova, and V. D. Myakushev, Thermochim. Acta **440**, 188 (2006).
[27] K. Karatasos, Macromolecules **38**, 4472 (2005).
[28] K. Karatasos, Macromolecules **39**, 4619 (2006).
[29] A. D. Meltzer, D. A. Tirrell, A. A Jones, P. T. Inglefield, D. M. Hedstrand, and D. A. Tomalia, Macromolecules **25**, 4541 (1992).
[30] M. H. Chai, Y. H. Niu, W. J. Youngs, and P. L. Rinaldi, J. Am. Chem. Soc. **123**, 4670 (2001).
[31] K. Karatasos, D. B. Adolf, and G. R. Davies, J. Chem. Phys. **115**, 5310 (2001).
[32] K. Vollmayr-Lee, W. Kob, K. Binder, and A. Zippelius, J. Chem. Phys. **116**, 5158 (2002).
[33] C. Kaur and S. Das, Phys. Rev. Lett. **89**, 085701 (2002).
[34] T. Forester and W. Smith, CCLRC, Daresbury Laboratory, Daresbury, Warrington Wa4 4AD, England. The simulations were performed by utilization of an appropriately modified version of the DL_POLY, package. DL_POLY is a parallel molecular dynamics package developed at Daresbury Laboratory, and is the property of the Council for the Central Laboratory of the Research Councils (CCLRC).
[35] S. Mayo, B. Olafson, and W. Goddard III, J. Phys. Chem. **94**, 8897 (1990).
[36] S. Havlin and D. Ben-Avraham, Adv. Phys. **36**, 695 (1987).
[37] M. Hurley and P. Harrowell, J. Chem. Phys. **105**, 10521 (1996).
[38] A. Blumen, C. von Ferber, A. Jurjiu, and T. Koslowski, Macromolecules **37**, 638 (2004).
[39] R. Zorn, J. Phys.: Condens. Matter **15**, R1025 (2003).
[40] S. Provencher, in *Photon Correlation Techniques in Fluid Mechanics*, edited by E. O. Schulz-DuBois (Springer-Verlag, Berlin, 1983), pp. 323–329.
[41] C. Bennemann, J. Baschnagel, and W. Paul, Eur. Phys. J. B **10**, 323 (1999).
[42] M. Aichele and J. Baschnagel, Eur. Phys. J. E **5**, 229 (2001).
[43] P. Allegrini, J. F. Douglas, and S. C. Glotzer, Phys. Rev. E **60**, 5714 (1999).
[44] F. Lindemann, Z. Phys. **11**, 609 (1910).
[45] J. Habasaki, K. L. Ngai, and Y. Hiwatari, Phys. Rev. E **66**, 021205 (2002).
[46] V. V. Hoang and S. K. Oh, J. Phys.: Condens. Matter **17**, 5179 (2005).
[47] J. Haile, *Molecular Dynamic Simulation: Elementary Methods* (Wiley, New York, 1997).